
Ultrarelativistic nucleus-nucleus collisions and the quark-gluon plasma

A. Andronic and P. Braun-Munzinger

Gesellschaft für Schwerionenforschung, Darmstadt, Germany

We present an overview of selected aspects of ultrarelativistic nucleus-nucleus collisions, a research program devoted to the study of strongly interacting matter at high energy densities and in particular to the characterization of the quark-gluon plasma (QGP). The basic features of the phase diagram of nuclear matter, as currently understood theoretically, are discussed. The experimental program, carried out over a broad energy domain at various accelerators, is briefly reviewed, with an emphasis on the global characterization of nucleus-nucleus collisions. Two particular aspects are treated in more detail: i) the application of statistical models to a phenomenological description of particle production and the information it provides on the phase diagram; ii) the production of hadrons carrying charm quarks as messengers from the QGP phase.

Go for the messes - that's where the action is.
S.Weinberg, Nature 426 (2003) 389

1 Introduction

Quantum Chromodynamics (QCD), the theory of strong interactions (see [1] for a recent review), predicts a phase transition from a state of hadronic constituents to a plasma of deconfined quarks and gluons, as the energy density exceeds a critical value. The opposite phase transition, from quarks and gluons to hadronic matter, took place about 10^{-5} s after the Big Bang, the primeval event which is at the origin of our Universe. The core of the physics program of ultrarelativistic nucleus-nucleus collisions research [2] is the study of the properties of strongly interacting matter at high energy density, in particular its phase diagram and the properties of quark-gluon plasma (QGP) [3].

Already in 1951 Pomeranchuk [4] conjectured that a finite hadron size implies a critical density, n_c , above which nuclear matter cannot be in a hadronic state. In 1965, Hagedorn [5] inferred that an exponentially growing mass spectrum of hadronic states (observed up to masses of about 1.5 GeV) implies a

critical temperature T_c of the order of 200 MeV ($\approx 2 \cdot 10^{12}$ K). However, the elementary building blocks of QCD, the quarks and gluons (carrying an extra quantum number called "color") have not been directly observed in experiments, although their fingerprints have been clearly identified in deep-inelastic collisions and jet production. A fundamental property of QCD, the asymptotic freedom, unraveled by Gross, Wilczek, and Politzer in 1973 [6], implies that the attractive force (coupling) between quarks increases as a function of their separation. Moreover, the confinement of quarks (and gluons) inside hadrons is another fundamental feature of QCD, although not fully understood yet. Cabibbo and Parisi [7] demonstrated already in 1975 that the exponential mass spectrum of hadronic states is a feature of any hadronic system which undergoes a second order phase transition with critical temperature T_c , since thermodynamical quantities exhibit singularities at T_c . This is realized in models that include "quark containment" [7], so is in agreement with QCD principles. Collins and Perry [8] demonstrated in the same year that asymptotically free QCD is also realized for large densities. It is interesting to note that ref. [7] contains the first sketch of a phase diagram of nuclear matter. The term quark-gluon plasma along with initial ideas about the space-time picture of hadronic collisions were first introduced by Shuryak [9].

2 Theoretical background

In the recent years, a successful effort to solve the QCD equations numerically on a (space-time) lattice has brought deeper insight into the subject of phase transition(s) from hadronic to quark-gluon matter [10]. It is not yet clear whether the transition is a true singular behaviour of thermodynamic variables or just a rapid crossover.

Fig. 1 shows a map of the phase transition in the coordinates of u, d and s quark masses and the chemical potential μ [10]. The surface, corresponding to a second order phase transition, is the border between the regions of first order transition and crossover. While the u and d quarks have small masses (of the order of a few MeV), the mass of the s quark is not well known, but is likely to be about 150 MeV. In this case (so-called physical values of the quark masses, represented by the vertical line in Fig. 1) the transition from QGP to a hadron gas is a crossover for small μ and reaches into the domain of the first order for large μ , implying the existence of a critical point [11]. Up to now, experimental searches for such a critical point via enhanced event-by-event fluctuations have not turned up any evidence [12]. Whether this means that all critical fluctuations are effectively damped by the phase transition or whether the transition is of first order, is currently an open question. It may also imply that the critical point is not reached in the energy range studied up to now.

In any case, the transition to free quarks and gluons is illustrated by the sudden increase of the energy density as a function of temperature, shown

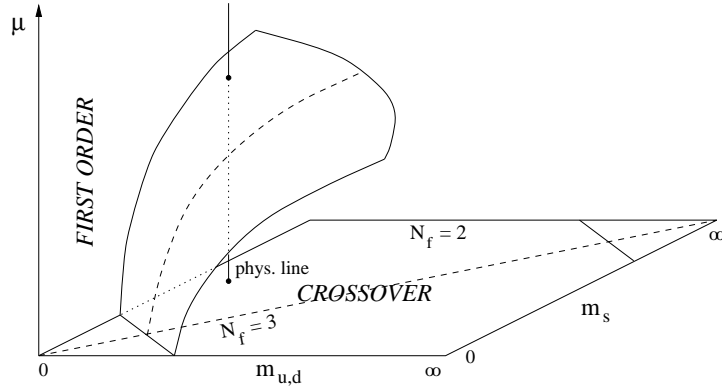


Fig. 1. Order of the phase transition in lattice QCD calculations in the variables quark masses (degenerate u , d quarks and s quark) and chemical potential (taken from ref. [10]).

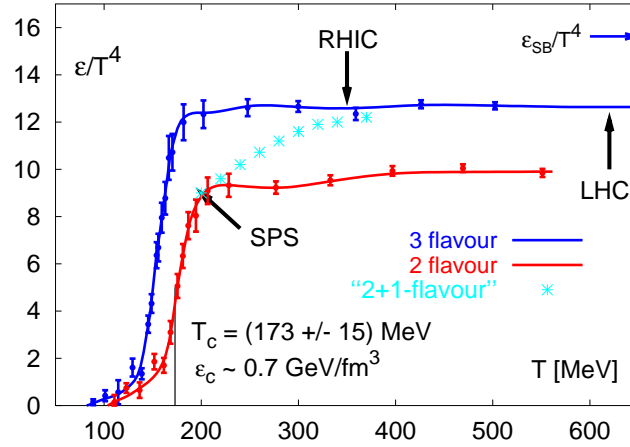


Fig. 2. Energy density as a function of temperature calculated with lattice QCD (taken from ref. [10]).

in Fig. 2 for two and three degenerate flavors [10]. For the 2-flavor case, the transition corresponds to a critical temperature $T_c \simeq 170$ MeV with critical energy density $\epsilon_c \simeq 0.7$ GeV, while for the 3-flavor case T_c is smaller by about 20 MeV. A result for the case of two degenerate flavors and a heavier strange quark (physical values) is also included.

Other features of Fig. 2 can be understood by recalling fundamental results of thermodynamics of relativistic gases [13]. The grand partition functions for fermions (particles and anti-particles) and bosons are:

$$(T \ln Z)_f = \frac{g_f V}{12} \left(\frac{7\pi^2}{30} T^4 + \mu^2 T^2 + \frac{1}{2\pi^2} \mu^4 \right), \quad (T \ln Z)_b = \frac{g_b V \pi^2}{90} T^4, \quad (1)$$

where g_f and g_b are the respective degeneracies (degrees of freedom). The average energy, particle number and entropy densities and the pressure are:

$$\varepsilon = \frac{T}{V} \frac{\partial(T \ln Z)}{\partial T} + \mu n, \quad n = \frac{1}{V} \frac{\partial(T \ln Z)}{\partial \mu}, \quad P = \frac{\partial(T \ln Z)}{\partial V}, \quad s = \frac{1}{V} \frac{\partial(T \ln Z)}{\partial T} \quad (2)$$

Using the thermodynamic relation: $\varepsilon = -P + Ts + \mu n$ one can easily establish the equation of state (EoS) of an ideal gas: $P = \varepsilon/3$. Assuming that the hadronic world is composed of pions, $g_h=3$. For three colours and two spin values, for quarks and gluons one has $g_q=12N_f$ and $g_g=16$, respectively. N_f is the number of flavours (the lighter quarks u , d and s are the only ones relevant). Consequently, at vanishing the chemical potential, the energy densities for the hadronic stage and for a gas of free quarks and gluons are, respectively:

$$\varepsilon_h/T^4 = \frac{\pi^2}{10}, \quad \varepsilon_{qg}/T^4 = (32 + 21N_f) \frac{\pi^2}{60}. \quad (3)$$

For $N_f=3$, $\varepsilon_{qg}/T^4=15.6$, denoted as the Stefan-Boltzmann limit, ε_{SB} , in Fig. 2. It is interesting to note that the calculated values are well below the values for non-interacting gases, indicating that the QGP is far from an ideal gas at temperatures as high as several times T_c .

An important (and not yet understood) result of lattice QCD calculations is that the critical temperatures for deconfinement and for chiral symmetry restoration (T_χ) apparently coincide, although one might expect that $T_\chi \geq T_c$ [10].

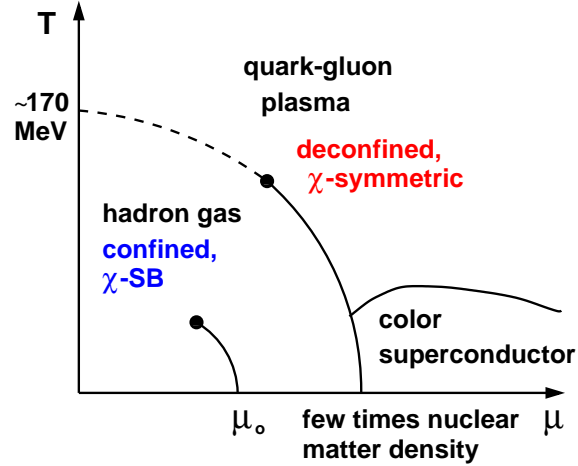


Fig. 3. Schematic phase diagram of nuclear matter (taken from ref. [10]).

A simple way to incorporate the two basic properties of QCD, asymptotic freedom and confinement, is achieved in the so-called (MIT) bag model [13]. It prohibits quarks and gluons from existing outside the bag (which can be any finite volume) by adding a shift from the physical vacuum into the QCD vacuum by an extra term in the partition function of the plasma phase: $(T \ln Z)_{vac} = -BV$, where B is the bag constant. It is easy to show that the EoS in this case becomes: $P = (\varepsilon - 4B)/3$. The phase transition trajectory in the $T - \mu$ plane can be constructed by applying the Gibbs criteria for the phase transition:

$$P_h = P_{qg}, \quad \mu_h = \mu_{qg}(= 3\mu_q), \quad T_h = T_{qg} = T_c. \quad (4)$$

A sketch of the present understanding [10] of the phase diagram of strongly interacting matter is shown in Fig. 3 in the $T - \mu$ plane, for two light u and d quarks and a heavy s quark. The lines mark the borders between the different phases of hadronic matter. The dots mark the expected position of critical points, namely the $T - \mu$ loci beyond which a first order phase transition is no longer expected to take place. Ground-state nuclear matter (atomic nuclei) corresponds to $\mu_0=931$ MeV (bound nucleon mass) and $T=0$ and is well modeled as a liquid. The line starting at this point denotes the liquid-gas phase boundary which is under study in low energy nucleus-nucleus collisions. The region of high temperatures is the part which is being explored in ultrarelativistic nucleus-nucleus collisions. The exotic region of low temperatures and high densities (high μ) is of relevance to astrophysical phenomena, but is rather likely to remain inaccessible to laboratory experiments.

3 Experimental program and global observables

By colliding heavy ions at ultrarelativistic energies, one expects to create matter under conditions that are sufficient for deconfinement [2]. A series of conferences (the so-called "Quark Matter" conferences, see ref. [15] for the most recent of those) devoted to the subject has begun in 1980 (Bielefeld).

The experimental program has started at the CERN's Super Proton Synchrotron (SPS) and at Brookhaven's Alternating Gradient Synchrotron (AGS) in 1985. The AGS program [16], carried out over a period of about 15 years by several experiments (E802/864,917 E810, E814/877, E864, E895) is essentially completed. The SPS program is just being concluded. Compelling evidence for the production of a "New State of Matter", has been produced in central Pb-Pb collisions [17] studied by seven experiments: WA80/98, NA35/49, NA38/50/60, NA44 NA45/CERES, WA97/NA57, and NA52. A vigorous research program, started with the first data taking in 2001, is on-going at the Relativistic Heavy Ion Collider (RHIC) at Brookhaven National Laboratory (BNL) [18] with four experiments, BRAHMS, PHENIX, PHOBOS and STAR. The Large Hadron Collider (LHC) will start operating at CERN in 2007 and

will provide (in addition to proton beams) heavy ion beams, which will be used in the research program of the dedicated ALICE experiment as well as by the ATLAS and CMS experiments [19]. A dedicated fixed-target facility is planned at Gesellschaft für Schwerionenforschung (GSI), expected to be operational in 2012 [20].

The temporal evolution of a (central) nucleus-nucleus collision at ultra-relativistic energies is understood to proceed through the following stages: i) liberation of quarks and gluons due to the high energy deposited in the overlap region of the two nuclei; ii) equilibration of quarks and gluons; iii) crossing of the phase boundary and hadronization; iv) freeze-out. Interesting experimental information is contained in the study of the distributions of (mostly charged) hadrons after freeze-out. Whether any information on the phase transition can be gleaned from these investigations will be discussed below. Clearly, given the short timescales of a nucleus-nucleus collision and the small volume involved (lattice QCD calculations discussed in the previous section are for bulk) the reconstruction of the various stages of the collision is a difficult task. It is consequently of particular relevance to find experimental observables which carry information (preferentially) from one particular stage, in particular about the QGP phase. Specific probes of QGP have been proposed [21, 22] and are currently being studied experimentally: i) direct photons [23]; ii) low-mass dileptons [24]; iii) strangeness [25]; v) charmonium suppression [3]; vi) jet-quenching [26]; vii) fluctuations [12, 27].

As shown in the next section, the study of hadron multiplicities in a statistical model is a unique way to provide experimental information on the QCD phase diagram [28]. Other global observables, like the distribution of particles over momentum space, collective flow, and the measurements of effective source sizes via particle interferometry, have also been studied in detail. In particular their energy evolution is of relevance and is briefly examined in the following ($\sqrt{s_{NN}}$ is the total center-of-mass energy per nucleon pair).

In Fig. 4 we present a compilation of experimental data on charged particle rapidity density distributions, dN_{ch}/dy , and transverse energy rapidity density, dE_T/dy , at midrapidity¹. The values are for central collisions (average value of the number of participant nucleons in the fireball, $N_{part}=350$, which roughly corresponds to the 5% most central collisions) in the energy range from AGS up to RHIC.² The continuous lines are $(\sqrt{s_{NN}})^{0.3}$ dependences, arbitrarily normalized. These power-law dependences describe the measurements quite well starting from the top AGS energy ($\sqrt{s_{NN}} \simeq 5$ GeV). This may suggest that some aspects of the underlying physics are similar over all this energy domain. Note that the SPS data (NA49) seem to slightly deviate from

¹ Midrapidity is the rapidity of center-of-mass system; rapidity is defined as $y = 0.5 \ln[(E + p_z)/(E - p_z)]$, where p_z is the longitudinal component of the particle momentum and E is the energy.

² A constant Jacobian of 1.1 has been used to convert the $dX/d\eta$ data to dX/dy . $\eta = -\ln[\tan(\theta/2)]$ is the pseudo-rapidity (θ is the polar angle of a given particle).

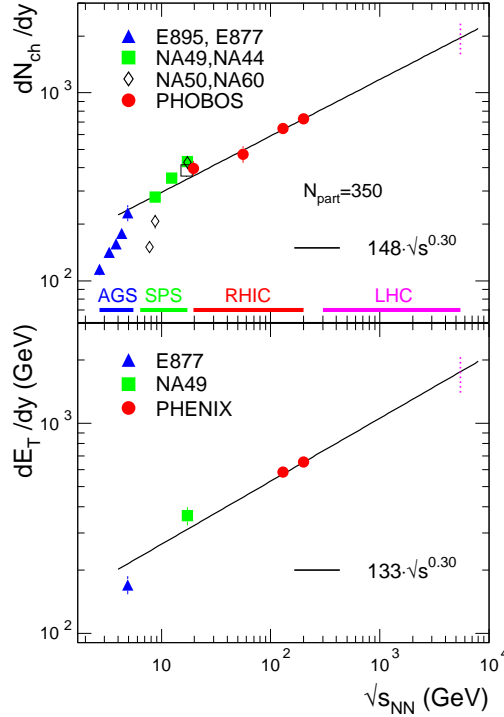


Fig. 4. Excitation function of global observables in central central nucleus-nucleus collisions ($N_{part}=350$). The experimental values for particle rapidity density, dN_{ch}/dy [29, 30, 31, 32, 33, 34, 35] (upper panel) and transverse energy rapidity density, dE_T/dy [30, 36] (lower panel) at midrapidity are plotted as symbols. The lines are a power law dependence arbitrarily scaled. The thick horizontal lines mark the energy range of the various accelerators. The dotted line marks the full LHC energy for Pb-Pb collisions ($\sqrt{s_{NN}}=5.5$ TeV).

the power-law behaviour. Also, at the lower SPS energies there is an apparent disagreement between NA49 and NA50/NA60 data. The $(\sqrt{s_{NN}})^{0.3}$ dependences allow for simple, experimentally-based, extrapolations to the LHC energy (of course, surprises are eagerly awaited). We note that power-law dependences are predicted by the (QCD-inspired) saturation model [37], but they are steeper (exponent 0.41, in case of dN_{ch}/dy). The steep decrease of particle multiplicities towards the lower end of the AGS energy range reflects mainly the threshold in the overall particle production, but may indicate a change in physics as well. The average transverse energy per charged particle has a nearly constant value of 0.8-0.9 GeV all the way from top AGS to RHIC energies.

The initial energy density, ε , and the net baryon density, n_{baryon} produced in a (central) heavy ion collision can be calculated from the measured transverse energy ($dE_T/d\eta$) and net baryon ($dN_{b-\bar{b}}/d\eta$) densities, respectively, in the so-called "Bjorken-scenario" [21]. This assumes self-similar (Hubble-like) homogeneous (hydrodynamical) expansion of the fireball in the longitudinal (beam) direction. The resulting relations are:

$$\varepsilon = \frac{1}{A_T} \frac{dE_T}{d\eta} \frac{d\eta}{dz}, \quad n_{baryon} = \frac{1}{A_T} \frac{dN_{b-\bar{b}}}{d\eta} \frac{d\eta}{dz} \quad (5)$$

where A_T is the transverse area of the fireball ($A_T = 154 \text{ fm}^2$ for a head-on Au-Au collision). In the above equations the only unknown parameter is the formation time (the time for establishing the equilibrium), τ ($d\eta/dz = 1/\tau$), which is usually taken to be $1 \text{ fm}/c$, although it is expected to decrease as a function of the energy. In this sense, the values obtained using Eq. 5 are conservative estimates for most of the energy range spanned by the experiments.

Table 1. Measured and deduced quantities at AGS, SPS, and RHIC for central nucleus-nucleus collisions. For the LHC case the values are extrapolations (see text).

Machine	AGS	SPS	RHIC	LHC
$\sqrt{s_{NN}}$ (GeV)	4.9	17.3	200	5500
$dE_T/d\eta$ (GeV)	192	363	625	1800 ?
$dN_{b-\bar{b}}/d\eta$	170	100	25	~ 0 ?
ε (GeV/fm ³)	1.2	2.4	4.1	11.6 ?
n_{baryon} (fm ⁻³)	1.1	0.65	0.17	?

The maximum nucleon-nucleon center-of-mass energy ($\sqrt{s_{NN}}$) and the corresponding measured and calculated (using Eq. 5) energy and baryon densities are listed in Table 1 for the various accelerator regimes. The results for LHC are extrapolations based on the $(\sqrt{s_{NN}})^{0.3}$ dependence discussed above.

The achieved densities are obviously very much larger than those inside a normal Pb nucleus: $\varepsilon_0 = 0.15 \text{ GeV}/\text{fm}^3$ and $n_0 = 0.16/\text{fm}^3$. The estimates of the energy densities are for all the energy range above the critical energy density at $\mu_b = 0$ ($\varepsilon_c \simeq 0.7 \text{ GeV}/\text{fm}^3$), indicating that the conditions for the QGP formation likely have been achieved in the experiments.

In Fig. 5 we present the excitation function of elliptic flow [38] for semi-central collisions (for which this observable has a maximum as a function of centrality). This observable is characterized by the second order Fourier coefficient $v_2 = \langle \cos(\phi) \rangle$, where ϕ is the azimuthal angle with respect to the reaction plane (defined by the impact parameter vector and the beam direction). It reflects the initial geometry of the overlap region and its pressure gradients. A transition from out-of-plane (also called "squeeze-out", $v_2 < 0$) to in-plane ($v_2 > 0$) preferential particle emission is seen in the energy domain of the AGS. This is the result of a combined effect of the violence of the expansion and of the shadowing of the spectator matter, which, at these energies is still present in the vicinity of the fireball. A striking correlation of this transition with the sharp increase of particle multiplicity at midrapidity (seen in Fig. 4) is evident. From top AGS energy up to RHIC the v_2 values increase steadily and are also well described by a $\log(\sqrt{s_{NN}})$ dependence. An early observation at RHIC was that the v_2 values are reaching the hydrodynamical [39] limits which is an indication of an early equilibration of the fireball. It is likely that QGP is the only way to achieve such a fast equilibration. It is thus an interesting question whether elliptic flow at LHC will follow the $\log(\sqrt{s_{NN}})$ trend or will flatten at the RHIC values.

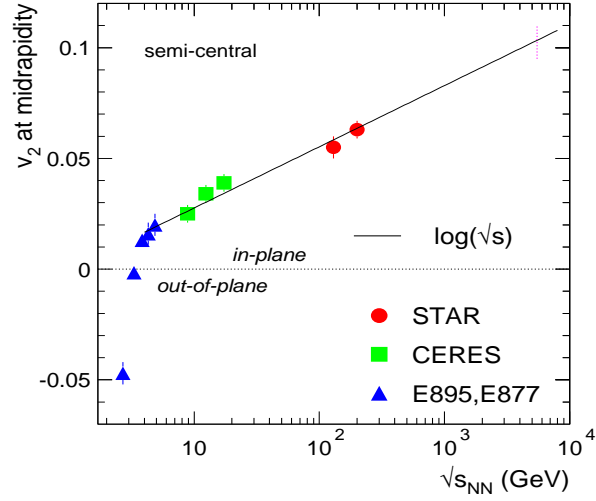


Fig. 5. Excitation function of elliptic flow. Protons are considered up to SPS energies and all charged particles at RHIC. The line is a $\log(\sqrt{s_{NN}})$ dependence arbitrarily normalized.

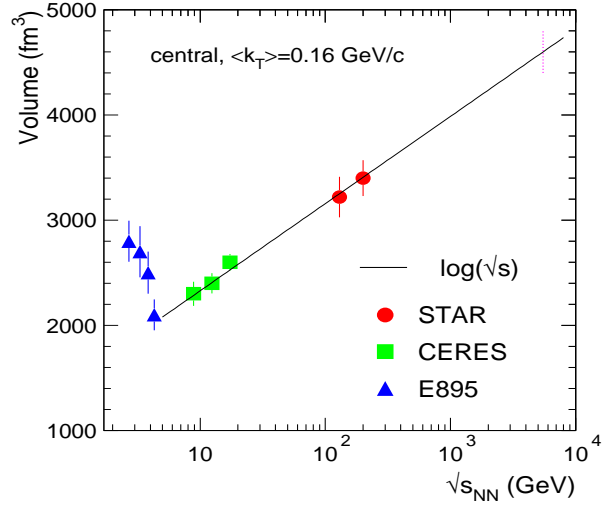


Fig. 6. Excitation function of the freeze-out volume extracted from pion HBT correlations. The line is a $\log(\sqrt{s_{NN}})$ dependence arbitrarily normalized.

In Fig. 6 we show the energy dependence of the volume of the fireball as extracted from pion Hanbury Brown-Twiss (HBT) correlations [40]. Again, a strikingly different behavior is seen at the lowest energies compared to top AGS and above, for which a $\log(\sqrt{s_{NN}})$ dependence describe the measure-

ments [41] well. This non-monotonic behavior can be understood [42] quantitatively as the result of an universal pion freeze-out at a critical mean free path $\lambda_f \simeq 1$ fm, independent of energy. It is worth mentioning that the smooth evolution of the source size in the energy range of top AGS to RHIC is an indication that no first order phase transition, associated with supercooling and explosive expansion, is visible in hadronic observables in this energy domain. Also, the measured source sizes at RHIC are well below hydrodynamic predictions.

4 Particle yields and their statistical description

The equilibrium behavior of thermodynamical observables can be evaluated as an average over statistical ensembles. The equilibrium distribution is thus obtained by an average over all accessible phase space. Furthermore, the ensemble corresponding to thermodynamic equilibrium is that for which the phase space density is uniform over the accessible phase space. In this sense, filling the accessible phase space uniformly is both a necessary and a sufficient condition for equilibrium. We restrict ourselves here on the basic features and essential results of the statistical model approach. A complete survey of the assumptions and results, as well as of the relevant references, is available in ref. [28].

The basic quantity required to compute the thermal composition of particle yields measured in heavy ion collisions is the partition function $Z(T, V)$. In the grand canonical (GC) ensemble, for particle i of strangeness S_i , baryon number B_i , electric charge Q_i and spin-isospin degeneracy factor $g_i = (2J_i + 1)(2I_i + 1)$, the partition function is:

$$\ln Z_i = \frac{V g_i}{2\pi^2} \int_0^\infty \pm p^2 dp \ln[1 \pm \exp(-(E_i - \mu_i)/T)] \quad (6)$$

with (+) for fermions (like baryons, made of 3 quarks) and (-) for bosons (like mesons, made of quark-antiquark pairs). Note that the partition functions introduced in Eq. 1 are for massless particles, for which the analytic integration of Eq. 6 can be performed. The particle density is:

$$n_i = N/V = -\frac{T}{V} \frac{\partial \ln Z_i}{\partial \mu} = \frac{g_i}{2\pi^2} \int_0^\infty \frac{p^2 dp}{\exp[(E_i - \mu_i)/T] \pm 1} \quad (7)$$

T is the temperature and $E_i = \sqrt{p^2 + m_i^2}$ is the total energy. $\mu_i = \mu_b B_i + \mu_S S_i + \mu_{I_3} I_{3i}$ is the chemical potential, with μ_B , μ_S , and μ_Q the chemical potentials related to baryon number, strangeness and electric charge, respectively, which ensure the conservation (on average) the respective quantum numbers: i) baryon number: $V \sum_i n_i B_i = Z + N$; ii) strangeness: $V \sum_i n_i S_i = 0$; iii) charge: $V \sum_i n_i I_{3i} = \frac{Z-N}{2}$. This leaves T and the baryochemical potential μ_b as the only parameters of the model. In practice, how-

ever, the volume determination may be subject to uncertainties due to incomplete stopping of the colliding nuclei. Due to this reason, the most convenient way to compare with measurements is to use particle ratios.

The interaction of hadrons and resonances is usually included by implementing a hard core repulsion of Van der Waals-type via an excluded volume correction. This is implemented in an iterative procedure according to:

$$P^{excl.}(T, \mu) = P^{id.gas}(T, \hat{\mu}); \quad \hat{\mu} = \mu - V_{eigen} P^{excl.}(T, \mu) \quad (8)$$

where V_{eigen} is calculated for a radius of 0.3 fm, considered identical for all particles.

The grand canonical ensemble is of course the simplest realization of a statistical approach and is suited for large systems, with large number of produced particles. However, for small systems (or peripheral nucleus-nucleus collisions) and for low energies in case of strangeness production, a canonical ensemble (C) treatment is mandatory. It leads to severe phase space reduction for particle production (so-called ‘‘canonical suppression’’). Within this approach, particle production in e^+e^- collisions has been successfully described, albeit with an additional heuristic strangeness suppression factor. It has been shown that the density of particle i with strangeness S calculated in the canonical approach, n_i^C , is related to the grand canonical value, n_i^{GC} , as: $n_i^C = n_i^{GC} F_S$, with $F_S = I_S(x)/I_0(x)$. The argument of the Bessel function of order S is the total yield of strange and antistrange particles. For central Pb-Pb (Au-Au) collisions, the canonical suppression is negligible for all strange particle species already for the highest AGS energy ($\sqrt{s_{NN}} \simeq 5$ GeV) but is sizeable for the lowest energy considered in the following, $\sqrt{s_{NN}} = 2.7$ GeV (corresponding to the beam energy of 2 GeV/n), for which $F_1 \simeq 2$, $F_2 \simeq 8$.

In Fig. 7 we present the result of a thermal fit of the measured particle ratios for Pb-Pb collisions at 158 GeV/nucleon beam energy. The values $T=170 \pm 5$ MeV and $\mu_b=255 \pm 10$ MeV are the free parameters. The reduced χ^2 (excluding ϕ and d) is 2.0, of which the largest contribution comes from the ratios Λ/π , Λ/h^- and Λ/K_s^0 , possibly due to weak decays feeding.

The thermal fits of particle ratios for the RHIC energies ($\sqrt{s_{NN}}=130$ and 200 GeV) are shown in Fig. 8. The obtained values for (T, μ_b) are $(174 \pm 7, 46 \pm 5)$ MeV and $(177 \pm 7, 29 \pm 6)$ MeV, respectively, with reduced χ^2 values of 0.8 and 1.1.

We mention here that the measured enhancement of strange hyperons (Λ , Ξ , Ω) at SPS in central Pb-Pb collisions with respect to pBe and pPb (a factor of 20 enhancement in case of Ω) can be understood quantitatively not as an enhancement in central Pb-Pb but as a suppression in pBe/pPb with respect to central Pb-Pb. It is also important to note that, at RHIC, the transverse momentum spectra can be well described in a thermal approach, with two additional (size) parameters [44]. At AGS, the measured yields of light nuclei ($A \leq 7$) are well explained by the thermal model [43].

T and μ_b were determined for other energies (SPS at 40 GeV/n, AGS at 10.8 GeV/n and for 1 GeV/n Au-Au collisions at SIS) with a similar fitting

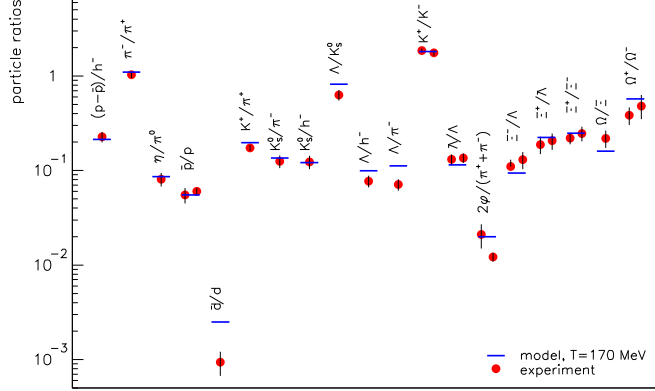


Fig. 7. Fit of particle ratios for Pb-Pb collisions at SPS (158 GeV/c). The measurements are the symbols, the thermal fit values are the lines.

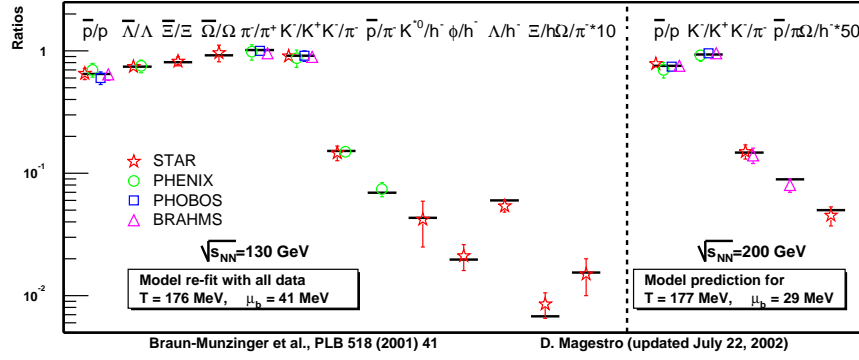


Fig. 8. Fit of particle ratios for Au-Au collisions at RHIC. The measurements are the symbols, the thermal model values are the lines.

procedure, although using in most cases fewer available measured ratios [28]. The resulting values are shown in a phase diagram of hadronic matter [43] in Fig. 9, together with calculations of freeze-out trajectories or a hadron gas at constant energy density and at constant baryon density. This latter case, corresponding to $n_b=0.12 \text{ fm}^{-3}$, does reproduce well the freeze-out points extracted from the data. Another observation is that the freeze-out points lie on a curve corresponding to an average energy $\langle E \rangle$ per average number of hadrons $\langle N \rangle$ of approximately 1 GeV. We have mentioned above that an universal pion freeze-out corresponding to a mean free path of about 1 fm has been derived from HBT source size measurements [42].

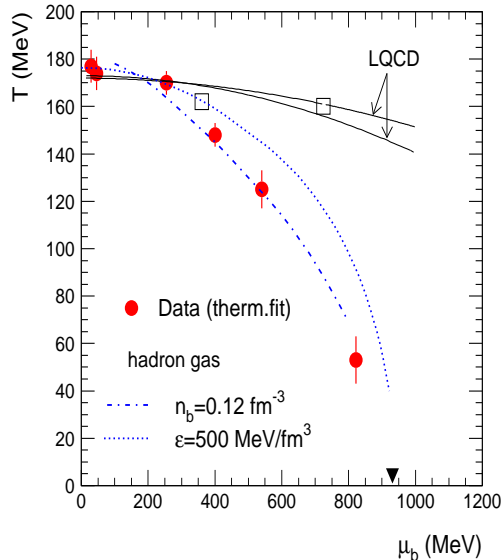


Fig. 9. The phase diagram of nuclear matter in the $T - \mu_b$ plane. The dots represent the extracted values from thermal fits to measured particle ratios. The trajectories of freeze-out for a hadron gas at constant energy density ($\epsilon=500 \text{ MeV}/\text{fm}^3$) and at constant baryon density ($n_b=0.12 \text{ fm}^{-3}$) are shown by the dotted and dash-dotted lines, respectively. The phase boundary from lattice QCD (LQCD) calculations is shown with continuous lines. The open squares indicate the critical point with two different inputs for calculations [11].

An important observation about the phase diagram is that, for the top SPS energy and above, the thermal parameters are (implying hadron yields frozen) at the phase boundary, as known from lattice QCD calculations [11]. A natural question though is how is equilibrium achieved? Considerations about collisional rates and timescales of the hadronic fireball expansion [45] imply that at SPS and RHIC the equilibrium cannot be established in the hadronic medium and that it is the phase transition which drives the particles densities and ensures chemical equilibrium.

In a recent paper [46] many body collisions near T_c were investigated as a possible mechanism for the equilibration. There it is argued that because of the rapid density change near a phase transition such multi-particle collisions provide a natural explanation for the observation of chemical equilibration at RHIC energies and lead to $T = T_c$ to within an accuracy of a few MeV. Any scenario with T substantially smaller than T_c would require that either multi-particle interactions dominate even much below T_c or that the two-particle cross sections are larger than in the vacuum by a high factor. Both of the latter hypothesis seem unlikely in view of the rapid density decrease. The critical temperature determined from RHIC for $T \approx T_c$ coincides well with lattice estimates [10] for $\mu = 0$, as discussed above. The same arguments as discussed here for RHIC energy also hold for SPS energies: it is likely that also there the phase transition drives the particle densities and ensures chemical equilibration.

We note that thermal models have also been used [47] to describe hadron production in e^+e^- and hadron-hadron collisions, leading to temperature pa-

rameters close to 170 MeV. This suggests that hadronization itself can be seen as a prethermalization process. However, to account for the strangeness undersaturation in such collisions, multi-strange baryons can only be reproduced by introducing a strangeness suppression factor of about 0.5, leading to a factor of 8 suppression of Ω baryons. This non-equilibrium feature, also visible in the momentum distributions of the produced particles, is most likely due to the "absence" of multi-particle scattering since the system is not in a high density phase due to a phase transition.

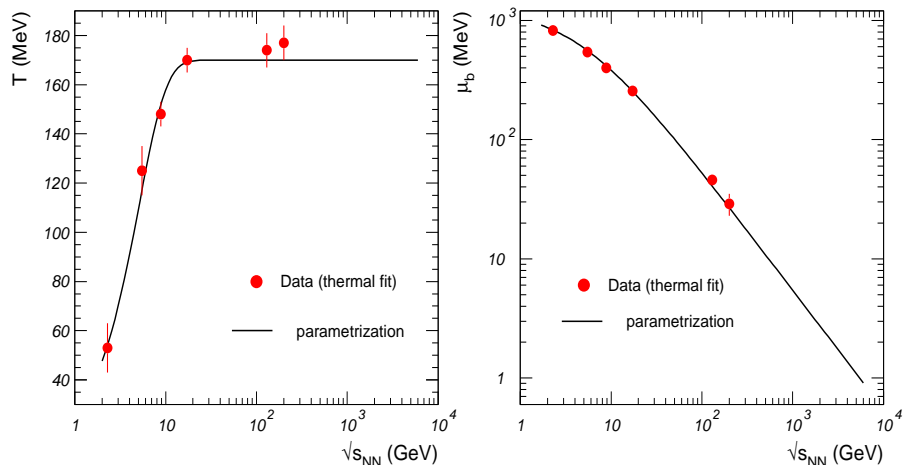


Fig. 10. Energy dependence of the thermal parameters T and μ_b . The symbols are the values extracted from experimental data, the lines are parametrizations (see text).

The energy dependence of the extracted T and μ_b values is presented in Fig. 10. The lines are parametrizations that allow for extrapolating the parameters up to the LHC energy. For μ_b the following parametrization has been used [28]:

$$\mu_b = 1270[\text{MeV}]/(1 + \sqrt{s_{NN}}[\text{GeV}]/4.3), \quad (9)$$

while T has been described with a Fermi-like function. For both cases the parametrizations describe well the extracted values over all the energy range.

In Fig. 11 we present excitation functions for a selection of strange particle yields over the whole energy range from lowest AGS to LHC energy. The experimental ratios K^\pm/π^\pm , Λ/π^+ and Ξ^-/Λ are calculated from measurements of absolute yields of π^\pm [29, 48, 31, 32, 49, 50], K^\pm [51, 31, 32, 49, 50], Λ [52] and Ξ^- [53]. The errors reflect the systematic uncertainties. These ratios are compared to thermal model calculations employing the parametrizations of T

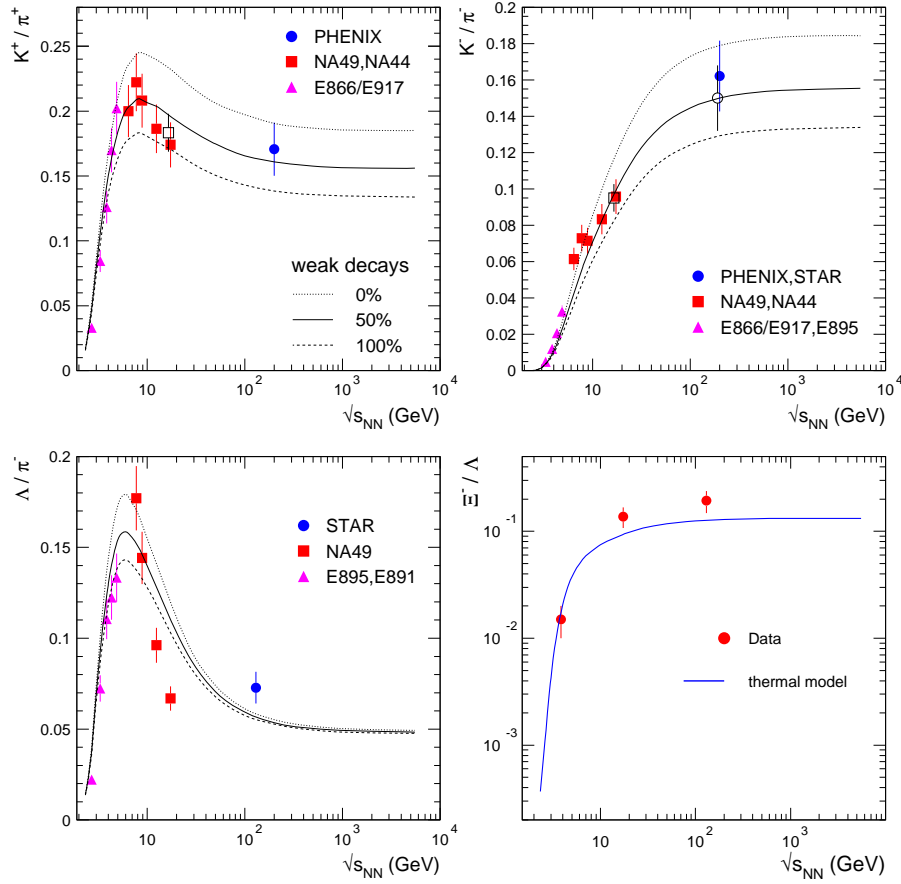


Fig. 11. Excitation function for strange particle production, K^\pm and Λ yields relative to pions, Ξ^- relative to Λ . All the measured data (symbols) are for midrapidity, with the exception of Λ and Ξ^- at AGS, for which only 4π yields are available. The lines are thermal model calculations for three cases of weak decay reconstruction efficiencies (see text).

and μ_b of Fig. 10. In case of the calculations the contribution (mainly important for pion yields) of down-feeding from resonances (via their weak decays) is taken into account in three different cases, assuming that none, 50% or all of the weak decays contribute to the yields. As one can see, the effect is significant, implying that it is very important that the experimental conditions (vertex cuts for selecting particles) for extracting the yields are well specified and taken into account in the model calculations. In a way, the extremes in weak decays reconstruction fraction shows the range of systematic uncertain-

ties that can arise in the comparison of model results with experimental data, if experimental information on feeding is ignored (or not known).

Given the accuracy of the description of multi-particle ratios presented above, it is not surprising that overall the model does reproduce the experimental values rather well up to RHIC energies. The observed discrepancies can be explained by the constant temperature (170 MeV) used for these calculations, which is not identical (although close) with the temperatures extracted from fits of multiparticle ratios shown above. An apparent disagreement between measurements and the model calculations is seen concerning the energy dependence of the K^+/π^+ and Λ/π^+ ratios at SPS energies. The origin of the rather narrow structure in the data is currently much debated [54]. We note that transport models also cannot reproduce the K^+/π^+ ratio [55].

The four ratios presented in Fig. 11 have a very different dependence on energy, which reflects the evolution of the fireball at freeze-out, dominated by the initial nucleons at low energies and by the newly created particles at RHIC and beyond. At LHC, it is expected that the fireball will consist exclusively of created particles. The steep variation of the ratios at the lowest energies reflects the close threshold for strangeness production. The canonical suppression plays an important role as well.

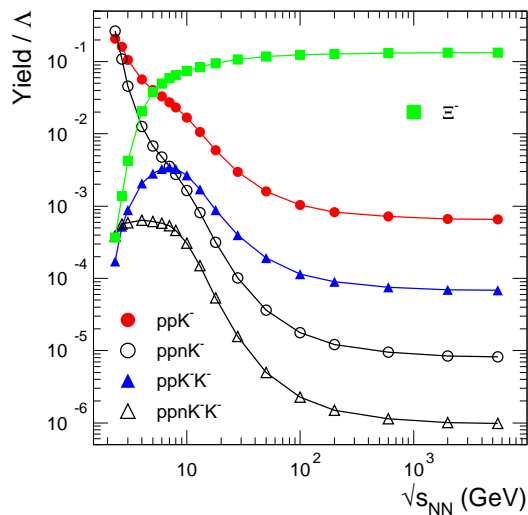


Fig. 12. Energy dependence of thermal yields of single and double K^- clusters relative to Λ . The yield of Ξ^- is included for reference.

With the T and μ_b values fixed by the fits to the measured particle ratios over a broad energy range, the thermal model has a good predictive power for all possible particles that can be formed at freeze-out. As an example, predictions for thermal yields of K^- clusters [56] relative to Λ hyperon are shown in Fig. 12 in comparison with the ratio Ξ^-/Λ . Such exotic K^- bound states have been predicted to form due to the strongly attractive K^- potential within nuclear matter [56], but are not yet observed experimentally. The

yield of single- K^- systems have large values, significantly above Ξ^- yields, at low energies and exhibit a pronounced decrease as a function of energy. The energy dependence of double- K^- systems exhibits a broad maximum around $\sqrt{s_{NN}} \simeq 6$ GeV, a region which will be covered by the future GSI accelerator [20].

In closing this section, we note that an open question remains concerning statistical model description of strongly decaying resonances (like ρ meson and Δ baryon). Their yields are strongly underestimated by the calculations [58, 28].

5 Charmonium and charmed hadrons

The importance of the so-called hard probes, among which the creation of heavy-quarks (c and b) have a prominent place, stems from the fact that they are exclusively created in primary hard collisions. Consequently, they are ideal messengers of the early stage (QGP phase) of the collision. In particular the J/ψ meson, which is a bound state of c and \bar{c} quarks, was predicted to melt in the quark-gluon plasma [3], thus providing a clear signature of its existence. Although recent theoretical investigations based on lattice QCD cast doubt on the melting at $T < 1.5T_c$ [57], there is continued interest in quarkonia as probes of the QGP.

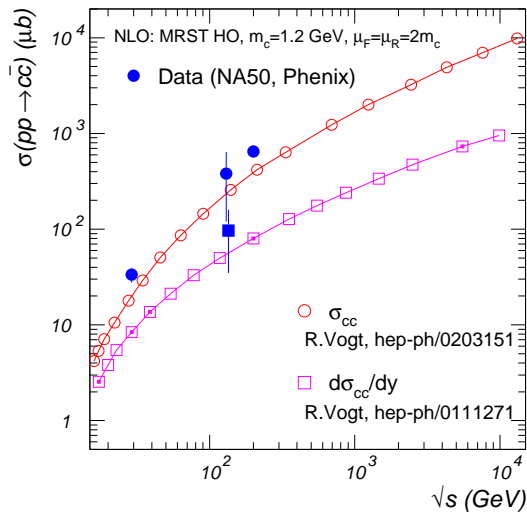


Fig. 13. Energy dependence of the total charm cross section in elementary (pp) collisions. The measurements performed with nucleus-nucleus experiments are compared to NLO pQCD calculations [62] for the integral and rapidity density cross section.

The production mechanisms of open charm (D mesons) and open beauty (B mesons) in elementary collisions can be well described by perturbative QCD (pQCD) calculations. For instance, data on charmed meson production

over a broad energy range was found [59] to be in good agreement with calculations using the PYTHIA code (in leading order approximation, so that a scale factor of 5 has been used in ref. [59] to approximate the next-to-leading order, NLO). Available experimental data on quarkonia production in pp collisions (J/ψ data for \sqrt{s} below 100 GeV and the Υ family data up to Tevatron energy, $\sqrt{s}=1.8$ TeV) have been successfully compared to pQCD calculations [60]. Recent measurements of J/ψ in pp collisions at RHIC are well described by (tuned) pQCD calculations, together with the measurements available at lower energies [61].

NLO pQCD calculations for total charm cross section in elementary collisions show clearly that the results depend significantly on the choice of several parameters, like the parton distribution function (PDF), charm quark mass (m_c) and renormalization and factorization constants, μ_R and μ_F [62]. This dependence is the bigger the larger the energy, so it is most crucial for LHC energies. A comparison of these calculations with data is presented in Fig. 13. With this choice of parameters, the calculations somewhat underpredict the measured values. Note that all the measurements are indirect: at SPS the cross section was estimated from the measured Drell-Yan cross section in pp [63], while at RHIC it was extracted from the charm contribution to the single-electron spectra measured in Au-Au collisions [64].

In nucleus-nucleus collisions, the J/ψ production at SPS is well measured by the NA50 collaboration [65] (see also ref. [66] for an in depth discussion). The measured ψ'/ψ ratio [67] is independent of energy and is in p-A collisions the same as in pp. This ratio is decreasing as a function of centrality in Pb-Pb collisions, as seen in Fig. 14 [67, 68], and reaches, for central collisions, a value expected for a thermal ensemble at $T \simeq 170$ MeV [69, 68]. For an interpretation of this result, see below.

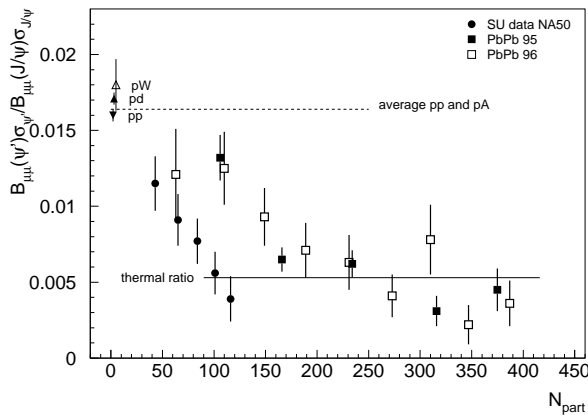


Fig. 14. Centrality dependence of the ratio $\psi'/(J/\psi)$ (including branching ratios into $\mu^+\mu^-$) at SPS.

At RHIC, the recent measurements of J/ψ [70] are hampered by very poor statistics, but high quality data are expected in the near future. First results on open charm production at RHIC in d-Au collisions have just been announced [71]. In the near future, open charm cross sections will be extracted from recently-completed measurements in In-In collisions by NA60 [34]. At LHC, there are good prospects to measure a complete set of charm and bottom particles [72], in particular with the ALICE experiment.

Below we discuss the QGP fingerprints as could be unraveled through the model of statistical hadronization of charm quarks [68]. A kinetic model description of J/ψ production has been independently developed [73]. It is equivalent from the point of view of the physical assumptions with the model discussed here, but differs in its numerical realization. Other approaches to statistical hadronization exist [74, 75], which differ from the model discussed here, but mostly in terms of inputs, while the outcome is qualitatively similar. The statistical hadronization model (we follow here the outline of ref. [76]) assumes that all charm quarks are produced in primary hard collisions and equilibrate³ in the quark-gluon plasma. An important corollary of this assumption is that no J/ψ mesons are preformed in the QGP, implying that the dissociation of J/ψ in QGP [3] is complete. As noted above, recent lattice QCD calculations show that the J/ψ mesons may not be dissociated in a deconfined medium below about $1.5T_c$ [57]. However, it is possible that, from SPS energy on, the initial temperature achieved in the collision exceeds this value.

The question of charm equilibration is a difficult one, but needs to be addressed. The cross sections for production of charmed hadrons are much too small [77] to allow for their chemical equilibration in a hadronic gas. But how can the apparently “thermal” values of the ratio ψ'/ψ be reconciled with this finding? We assume that all charm quarks are produced in initial hard collisions, but that open and hidden charm hadrons are formed at chemical freeze-out according to statistical laws. Consistent with the fact that, at the top SPS energy and beyond, chemical freeze-out appears to be at the phase boundary (see previous section), the model implies that a QGP phase was a stage in the evolution of the fireball. The analysis of J/ψ spectra at SPS [78] lends further support to the statistical hadronization picture where J/ψ decouples at chemical freeze-out. A recent analysis of single-electron spectra at RHIC [79] also strengthens the case for an early thermalization of heavy quarks. However, in that analysis it was pointed out that both the hydrodynamical approach and PYTHIA reproduce the measured single-electron spectra, although the two approaches are different in detail at low p_t and differ manifestly at high p_t ($p_t \gg$ mass of charm quark). Another theoretical analysis [80] indicates though that charm quarks might not thermalize quickly because of their large mass. All of this emphasizes the need to have high-

³ This implies thermal, but not chemical equilibrium for charm quarks.

precision direct measurements of open charm, which could impose constraints on different interpretations.

In statistical models charm production needs to be treated within the framework of canonical thermodynamics [28]. Thus, the charm balance equation required during hadronization is expressed as:

$$N_{c\bar{c}}^{dir} = \frac{1}{2}g_c N_{oc}^{th} \frac{I_1(g_c N_{oc}^{th})}{I_0(g_c N_{oc}^{th})} + g_c^2 N_{c\bar{c}}^{th}. \quad (10)$$

Here $N_{c\bar{c}}^{dir}$ is the number of directly produced $c\bar{c}$ pairs and I_n are modified Bessel functions. In the fireball of volume V the total number of open $N_{oc}^{th} = n_{oc}^{th}V$ and hidden $N_{c\bar{c}}^{th} = n_{c\bar{c}}^{th}V$ charm hadrons are computed from their grand-canonical densities n_{oc}^{th} and $n_{c\bar{c}}^{th}$, respectively. The densities of different particle species in the grand canonical ensemble are calculated following the statistical model [28] introduced in the previous section. All known charmed mesons and hyperons and their decays are included in the calculations.

The balance equation (10) defines a fugacity parameter g_c that accounts for deviations of charm multiplicity from the value that is expected in complete chemical equilibrium. The yield of open charm mesons and hyperons i and of charmonia j is obtained from:

$$N_i = g_c N_i^{th} \frac{I_1(g_c N_{oc}^{th})}{I_0(g_c N_{oc}^{th})} \quad \text{and} \quad N_j = g_c^2 N_j^{th}. \quad (11)$$

The above model for charm production and hadronization can be only used if the number of participating nucleons N_{part} is sufficiently large. Taking into account the measured dependence of the relative yield of ψ' to J/ψ on centrality in Pb–Pb collisions at SPS energy, seen in Fig. 14, the model appears appropriate for $N_{part} > 100$, for which the ratio approaches the thermal value [69, 68].

To calculate the yields of open and hidden charm hadrons for a given centrality and collision energy one needs to fix a set of parameters in Eq.(10) and (11):

i) A constant temperature of 170 MeV and a baryonic chemical potential μ_b according to the parametrization (9) are used for our calculations (see Fig 10). These thermal parameters are consistent with those required to describe experimental data on different hadron yields for SPS and RHIC energies.

ii) The volume of the fireball. We focus on rapidity density calculations which are of relevance for the colliders, so in this case the volume corresponds to a slice of one rapidity unit at midrapidity, $V_{\Delta y=1}$. It is obtained from the charged particle rapidity density dN_{ch}/dy , via the relation $dN_{ch}/dy = n_{ch}^{th} V_{\Delta y=1}$, where n_{ch}^{th} is the charged particle density computed within the thermal model. The charged particle rapidity densities (and total yields in case of SPS, for which we calculate 4π yields for a direct comparison to experimental data) are taken from experiments at SPS and RHIC and

extrapolated to LHC energy (as seen in Fig. 4). Central collisions correspond to $N_{part}=350$. For the centrality dependences we assume that the volume of the fireball is proportional to N_{part} .

Table 2. Input (dN_{ch}/dy and $dN_{c\bar{c}}^{dir}/dy$) and output ($V_{\Delta y=1}$ and g_c) parameters for model calculations at top SPS, RHIC and LHC for central collisions ($N_{part}=350$).

$\sqrt{s_{NN}}$ (GeV)	17.3	200	5500
dN_{ch}/dy	430	730	2000
$dN_{c\bar{c}}^{dir}/dy$	0.064	1.92	16.8
$V_{\Delta y=1}$ (fm ³)	861	1663	4564
g_c	1.86	8.33	23.2

iii) The yield of open charm $dN_{c\bar{c}}^{dir}/dy$ at midrapidity (or in full volume) is taken from NLO pQCD calculations for pp collisions [62] and scaled to nucleus-nucleus collision via the nuclear overlap function, T_{AA} [81]. For a given centrality:

$$\frac{dN_{c\bar{c}}^{dir}}{dy}(N_{part}) = \frac{d\sigma(pp \rightarrow c\bar{c})}{dy} T_{AA}(N_{part}). \quad (12)$$

The pQCD calculations with the MRST HO PDF are used here.

The input values dN_{ch}/dy and $dN_{c\bar{c}}^{dir}/dy$ and the corresponding volume at midrapidity and enhancement factor are summarized in Table 2 for model calculations for different collision energies.

We first compare predictions of the model to 4π -integrated J/ψ data at the SPS measured by NA50 collaboration [65, 82]. For the fireball total volume $V=3070$ fm³ (for $N_{ch} = 1533$) the total yield of thermal open charm pairs is $N_{oc}^{th}=0.98$. This is to be contrasted with $N_{c\bar{c}}^{dir}=0.137$ from NLO calculations [62], leading to a value of $g_c=0.78$. Although g_c is here close to unity, this obviously does not indicate that charm production appears at chemical equilibrium, as the suppression factor is a strongly varying function of the collision energy. We have already indicated that, within the time scales available in heavy ion collisions, the chemical equilibration of charm is very unlikely both in confined and deconfined media.

In Fig. 15 we show the comparison between the results of our model and NA50 data for two different values of $N_{c\bar{c}}^{dir}$: from NLO calculations [62] and scaled up by a factor of 2.8. Using the NLO cross sections for charm production scaled by the nuclear overlap function, the model underestimates the measured yield. To explain the overall magnitude of the data, we need to increase the $N_{c\bar{c}}^{dir}$ yield by a factor of 2.8 as compared to NLO calculations. We mention in this context that the observed [63] enhancement of the di-muon yield at intermediate masses has been interpreted as a possible indication for an anomalous increase of the charm production cross section. A third calculation (resulting in the dash-dotted line in Fig. 15) is using the NLO cross section scaled-up

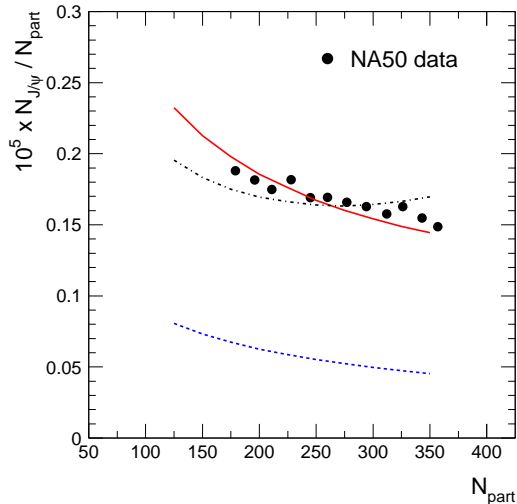


Fig. 15. The centrality dependence of J/ψ production at SPS. Model predictions are compared to 4π -integrated NA50 data [65, 82]. Two curves for the model correspond to the values of $N_{c\bar{c}}^{dir}$ from NLO calculations (dashed line) and scaled up by a factor of 2.8 (continuous line). The dash-dotted curve is obtained when considering the possible NA50 N_{part} -dependent charm enhancement over their extracted pp cross section [63] (see text).

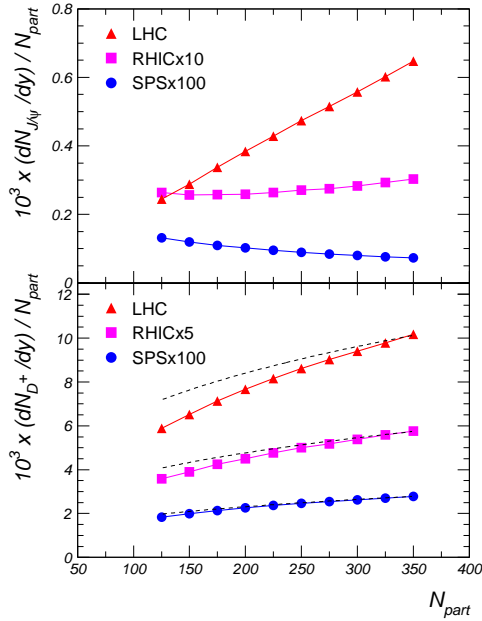
by 1.6, which is the ratio of the open charm cross section estimated by NA50 for pp collisions at 450 GeV/c [63] and the present NLO values. For this case the N_{part} scaling is not the overlap function, but is taken according to the measured di-muon enhancement as a function of N_{part} [63]. The resulting J/ψ yields from the statistical model are on average in agreement with the data, albeit with a flatter centrality dependence than by using the nuclear overlap function. Thus our charm enhancement factor of 2.8 needed to explain the J/ψ data is very similar to the factor needed to explain the intermediate mass dilepton enhancement assuming that it arises exclusively from charm enhancement [63]. We note, however, that other plausible explanations exist of the observed enhancement in terms of thermal radiation [83].

We turn now to discuss our model predictions for charmonia and open charm production at collider energies and compare them with the results obtained at SPS. Notice that from now on we focus on rapidity densities, which are the relevant observables at the colliders. In Table 3 we summarize the yields for a selection of hadrons with open and hidden charm. All predicted yields increase strongly with beam energy, reflecting the increasing charm cross section and the concomitant importance of statistical recombination. Also, ratios of open charm hadrons evolve with increasing energy, reflecting the corresponding decrease in the charm chemical potential. Very recent measurements of open charm in d-Au collisions at RHIC [71] yield the ratio $(D^{*+} + D^{*-}) / (D^0 + \bar{D}^0)$ of 0.40 ± 0.09 , which is in a good agreement to the model prediction of 0.42.

Model predictions for the centrality dependence of J/ψ and D^+ rapidity densities normalized to N_{part} are shown in Fig. 16. The results for J/ψ mesons exhibit, in addition to the dramatic change in magnitude, a striking

Table 3. Mid-rapidity densities for open and hidden charm hadrons, calculated for central collisions ($N_{part}=350$) at SPS, RHIC and LHC.

$\sqrt{s_{NN}}$ (GeV)	17.3	200	5500
D^+	0.010	0.404	3.56
D^-	0.016	0.420	3.53
D^0	0.022	0.888	7.80
\bar{D}^0	0.035	0.928	7.82
D^{*+}	0.009	0.374	3.30
D^{*-}	0.015	0.393	3.30
D_s^+	0.012	0.349	2.96
D_s^-	0.009	0.338	2.95
A_c	0.014	0.153	1.16
\bar{A}_c	0.0012	0.117	1.15
J/ψ	$2.55 \cdot 10^{-4}$	0.011	0.226
ψ'	$0.95 \cdot 10^{-5}$	$3.97 \cdot 10^{-4}$	$8.46 \cdot 10^{-3}$


Fig. 16. Centrality dependence of rapidity densities of J/ψ (upper panel) and D^+ (lower panel) mesons per N_{part} at SPS, RHIC and LHC. Note the scale factors for RHIC and SPS energies. The dashed lines in the lower panel represent $N_{part}^{1/3}$ dependences normalized for $N_{part}=350$.

change in the shape of the centrality dependence. In terms of the model this change is a consequence of the transition from the canonical to the grand-canonical regime. For D^+ -mesons, the expected approximate scaling of the ratio $D^+/N_{part} \propto N_{part}^{1/3}$ (dashed lines in Fig. 16) is only roughly fulfilled due to departures of the nuclear overlap function from the simple $N_{part}^{4/3}$ dependence.

The results summarized in Table 3 and shown in Fig. 16 obviously depend on two input parameters, dN_{ch}/dy and $dN_{c\bar{c}}^{dir}/dy$. For LHC energy, neither one of these parameters is well known. An increase of charged particle multiplicities by up to a factor of three beyond our “nominal” value $dN_{ch}/dy=2000$ for central collisions is conceivable. However, due to quite large uncertainties on the amount of shadowing at LHC energy, these results may be still modified. The yield of $dN_{c\bar{c}}^{dir}/dy$ is also not well known at LHC energy. Although these uncertainties affect considerably the magnitude of the predicted yields, their centrality dependence remains qualitatively unchanged: the yields per participant are increasing functions of N_{part} . We also note here that, while detailed predictions differ significantly, qualitatively similar results (see ref. [72]) have been obtained for a kinetic model study of J/ψ production at the LHC.

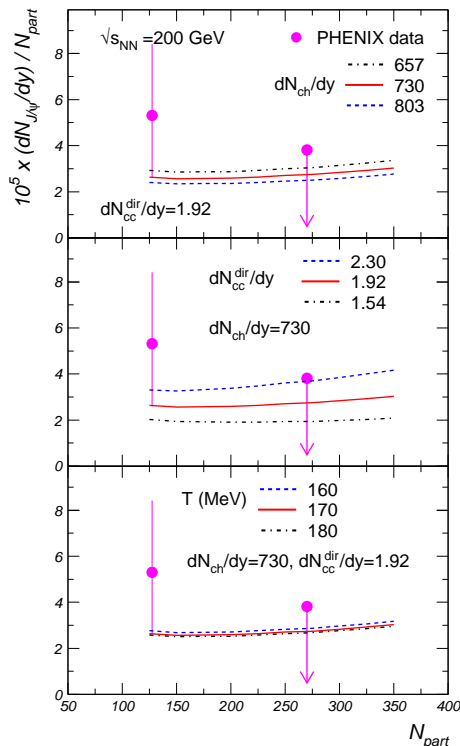


Fig. 17. Centrality dependence of rapidity densities of J/ψ mesons at RHIC. Upper panel: sensitivity to dN_{ch}/dy ; middle panel: sensitivity to $dN_{c\bar{c}}^{dir}/dy$; lower panel: sensitivity to T . The calculations are represented by lines. The dots are experimental data from the PHENIX collaboration [70]. Note that the point for the central collisions is the upper limit extracted by PHENIX for 90% C.L. [70].

In Fig. 17 we present the predicted centrality dependence of the J/ψ rapidity density normalized to N_{part} for RHIC energy ($\sqrt{s_{NN}}=200$ GeV). The three panels show its sensitivity on dN_{ch}/dy , $dN_{c\bar{c}}^{dir}/dy$, and (freeze-out) temperature T . The calculations are compared to experimental results of the PHENIX Collaboration [70]. The experimental data have been rescaled according to our procedure to calculate N_{part} and the number of binary collisions, N_{coll} . Within

the still large experimental error bars, the measurements agree with our model predictions. In Fig. 17 only the statistical errors of the mid-central data point are plotted. The systematic errors are also large [70]. A stringent test of the present model can only be made when high statistics J/ψ data are available.

We turn now to a more detailed discussion of the sensitivity of our calculations to the various input parameters as quantified in Fig. 17. First we consider the influence of a 10% variation of dN_{ch}/dy on the centrality dependence of J/ψ yield. Note that the total experimental uncertainty of dN_{ch}/dy (which is for the moment the measured observable for most experiments) at RHIC is below 10%. The sensitivity on the dN_{ch}/dy values stems from the volume into which the (fixed) initial number of charm quarks is distributed. The smaller the particle multiplicities and thus also the fireball volume, the more probable it is for charm quarks and antiquarks to combine and form quarkonia. That is why one sees, in the top panel in Fig. 17, that the J/ψ yield is increasing with decreasing charge particle multiplicity.

The sensitivity of the predicted J/ψ yields on $dN_{c\bar{c}}^{dir}/dy$ is also straightforward. The larger this number is in a fixed volume the larger is the yield of charmed hadrons. In case of charmonia the dependence on $dN_{c\bar{c}}^{dir}/dy$ is non-linear due to their double charm quark content, as reflected by the factor g_c^2 in equation (11). To illustrate the sensitivity of the model predictions on $dN_{c\bar{c}}^{dir}/dy$, we exhibit the results of a 20% variation with respect to the value given in Table 2. The open charm cross section is not yet measured at RHIC. However, some indirect measurements can be well reproduced, within the experimental errors, by PYTHIA calculations using a p-p charm cross sections scaled with the number of collisions N_{coll} of $650 \mu b$ [64]. The corresponding value at $\sqrt{s_{NN}}=130$ GeV is $330 \mu b$ [64]. For comparison, the NLO pQCD values we are using are 390 and $235 \mu b$, respectively. Despite the still large experimental uncertainties, this discrepancy needs to be understood. We note that, dependent on the input parameters used in the NLO calculations [62], possible variations of the open charm production cross section for the RHIC energy are of the order of $\pm 20\%$. In terms of our model this variation corresponds to about a $\pm 30\%$ change of the J/ψ yield, which is also centrality dependent (see middle panel in Fig. 17). If we use the PHENIX p-p cross section of $650 \mu b$, the calculated yield is a factor 2.5 larger for $N_{part}=350$ and increases somewhat stronger with centrality. As apparent in Fig. 17, the predictive power of this model, or of any similar model, relies heavily on the accurate knowledge of the charm production cross section. A simultaneous description of the centrality dependence of open charm together with J/ψ production is, in this respect, mandatory to test the concept of the statistical origin of open and hidden charm hadrons in heavy ion collisions at relativistic energies.

The apparent weak dependence of J/ψ yield on freeze-out temperature, seen in Fig. 17, may be surprising. In our model this result is a consequence of the charm balance equation (11). The temperature variation leads, obviously, to a different number of thermally produced charmed hadrons, but this is

compensated by the g_c factor. The approximate temperature dependence of g_c and the J/ψ yield are:

$$g_c(T) \sim 1/N_D^{th} \sim e^{\frac{m_D}{T}}, \quad N_{J/\psi}(T) = g_c^2 N_{J/\psi}^{th} \sim e^{\frac{2m_D - m_{J/\psi}}{T}} \quad (13)$$

As a result of the small mass difference in the exponent the J/ψ yield exhibits only a weak sensitivity on T . This is in contrast to the purely thermal case where the yield scales with $\exp(-m_{J/\psi}/T)$. The only exception is the ratio $\psi'/J/\psi$, which is obviously identical in the statistical hadronization scenario and in the thermal model and coincides, for $T \simeq 170$ MeV, with the measured value at SPS (see Fig. 14).

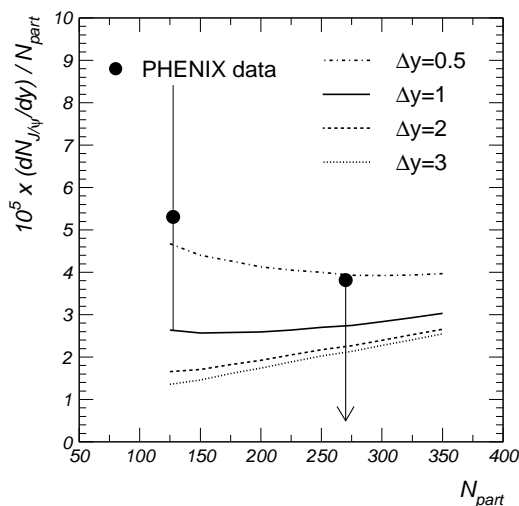


Fig. 18. Centrality dependence of rapidity densities of J/ψ mesons at RHIC for different rapidity window sizes. The lines are calculations, the dots are experimental data from PHENIX collaboration [70] (the point for the central collisions is the upper limit for 90% C.L.).

Most of our results presented above are obtained considering a one unit rapidity window at midrapidity, while results for the full volume were presented only for the SPS. Unlike the kinetic model of Thews et al. [73], our model does not contain dynamical aspects of the coalescence process. However, in our approach, the width of the rapidity window does influence the results in the canonical regime. For the grand-canonical case, attained only at LHC energy, there is no dependence on the width of the rapidity window, due to a simple cancellation between the variation of the volume, proportional to the rapidity slice in case of a flat rapidity distribution, and the variation of $N_{c\bar{c}}^{dir}$, also proportional to the width of the rapidity slice. In Fig. 18 we present the centrality dependence of J/ψ rapidity densities for RHIC energy and for different rapidity windows Δy from 0.5 to 3. The dependence on Δy resembles that of the kinetic model [73], but is less pronounced. The available data are not yet precise enough to rule out any of the scenarios considered.

However, for the kinetic model, the cases of small Δy seem to be ruled out by the present PHENIX data. We stress in this context that the size of the Δy window has a potentially large impact on the results at SPS energy. It is conceivable that no charm enhancement is needed to explain the data if one considers a sufficiently narrow rapidity window for the statistical hadronization.

Particle	Statistical hadronization	pQCD NLO
D^+	0.228	0.155
D^-	0.226	0.146
D_s^+	0.190	0.095
D_s^-	0.189	0.089
Λ_c	0.074	0.086
$\bar{\Lambda}_c$	0.074	0.062

Table 4. Ratios of midrapidity densities for open charm hadrons relative to $(D^0 + \bar{D}^0)$, calculated for central collisions at LHC. The results of the statistical hadronization model are compared to NLO pQCD calculations [72].

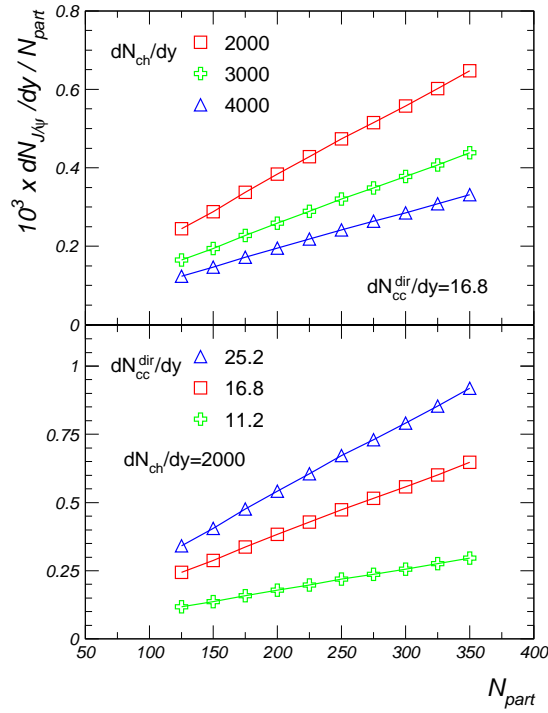


Fig. 19. Centrality dependence of rapidity densities of J/ψ (per N_{part}) at LHC. Upper panel: sensitivity to dN_{ch}/dy , lower panel: sensitivity to dN_{cc}^{dir}/dy .

Ratios of mid-rapidity densities for open charm hadrons relative to ($D^0 + \bar{D}^0$) are presented in Table 4 for central collisions at LHC. The statistical hadronization model results are compared to NLO pQCD calculations [72]. In case of pQCD, the production of charm is identical to the elementary case, namely charm quark production in hard processes. Sizeable differences (up to a factor of 2, in case of D_s mesons) are seen. The measurements will certainly be able to distinguish between the two scenarios.

In Fig. 19 we present the statistical hadronization model results on rapidity densities of J/ψ per N_{part} for the LHC energy. We study the sensitivity on the two input parameters that are not well known at LHC, dN_{ch}/dy and $dN_{c\bar{c}}^{dir}/dy$. Within the variations considered here (up to a factor 2 larger particle multiplicities and a $\pm 50\%$ in the charm cross section) the changes in the yields are considerable, but the dependences on N_{part} remain the same, making this a rather solid prediction for LHC.

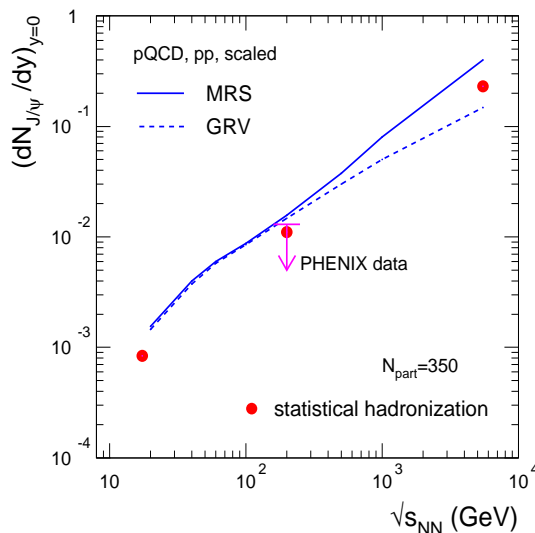


Fig. 20. Excitation function of J/ψ production in central nucleus-nucleus collisions. The symbols are statistical hadronization model calculations. The lines are pQCD calculations for pp collisions [60], scaled for $N_{part}=350$, for two PDFs. The arrow denotes the experimental value [70].

The excitation function of J/ψ production (rapidity densities) is shown in Fig. 20. The statistical hadronization model results are compared to pQCD calculations for pp collisions [60], scaled for $N_{part}=350$, for two PDFs. Note that the PDFs, as well as the other inputs of the pQCD calculations [60] are different from those used to extract the charm cross section [62] which is an input to the statistical hadronization model. In any case, the yields are comparable in the two cases, implying that fine tuning of the input values will be needed to be able to distinguish between the two scenarios. As in the case of the total charm cross section [62], the dependence of J/ψ production on the PDF choice is evident for the higher energies (LHC).

The results presented above were obtained under the assumption of statistical hadronization of quarks and gluons. We have assumed that charm quarks are entirely produced via primary hard scattering and thermalized in the QGP. No secondary production of charm in the initial and final state was included in our calculations. Final state effects like nuclear absorption of J/ψ [3] are also neglected. First RHIC data on J/ψ production support the current predictions, although the experimental errors are for the moment too large to allow firm conclusions. Also the RHIC results on open charm lend a strong support for this model. The statistical coalescence implies travel of charm quarks over significant distances e.g. in a QGP. If the model predictions will describe consistently precision data this would be a clear signal for the presence of a deconfined phase. We emphasize that the predictive power of this (and any similar) model relies heavily on the accuracy of the charm cross section, which is yet to be directly measured in nucleus-nucleus collisions.

6 Outlook

The field of ultrarelativistic nucleus-nucleus collisions has reached the stage of precision measurements, which are able to provide fundamental information on the strongly interacting matter at high temperature and (energy) density and in particular on the quark-gluon plasma. It is now clear that such complex knowledge can only be achieved by a set of multi-faceted and complementary studies and that no one single observable is sufficient to characterize fully the properties of the QGP phase. From what we have briefly reviewed here it is clear that the global characterization of the collision has been convincingly achieved and, subject to further refinements, establishes beyond doubt that the conditions for the creation of QGP have been attained. We have shown that the study of particle ratios provide unique insight on the QCD phase diagram, while the study of charm hadrons provides a valuable glimpse into the QGP.

We look forward to new high statistics and precision experiments from the SPS and, in particular, RHIC. From 2007 on the high temperature region of the phase diagram will be investigated in detail at the LHC with the dedicated ALICE experiment as well as within the ATLAS and CMS collaborations. The next serious attack on the high density-moderate temperature regime will be addressed further in the future with the new GSI accelerator facility. Interesting times are ahead!

References

1. F. Wilczek, hep-ph/0003183; D.E. Kharzeev, J. Raufeisen, nucl-th/0206073.
2. See e.g. H. Satz, Nucl. Phys. A 715 (2003) 3 [hep-ph/0209181] and ref. therein.
3. H. Satz, Rep. Prog. Phys. 63 (2000) 1511 [hep-ph/0007069].

4. I.Ya. Pomeranchuk, Dokl. Akad. Nauk. SSSR 78 (1951) 889.
5. R. Hagedorn, Nuovo Cim. Suppl. 3 (1965) 147; see also: T. Ericson, J. Rafelski, CERN Courier 43, Nr.7 (2003) 30.
6. D.J. Gross, F. Wilczek, Phys. Rev. Lett. 30 (1973) 1343; H.D. Politzer, Phys. Rev. Lett. 30 (1973) 1346.
7. N. Cabbibo, G. Parisi, Phys. Lett. B59 (1975) 67.
8. J.C. Collins, M.J. Perry, Phys. Rev. Lett. 34 (1975) 1353.
9. E.V. Shuryak, Phys. Lett. B 78 (1978) 150.
10. F. Karsch, Lect. Notes Phys. 583 (2002) 209 [hep-lat/0106019]; F. Karsch, E. Laermann, hep-lat/0305025; E. Laermann, O. Philipsen, hep-ph/0303042.
11. Z. Fodor, S.D. Katz, J. High En. Phys. 203 (2002) 14 [hep-lat/0106002], [hep-lat/0402006]; P. de Forcrand, O. Philipsen, Nucl. Phys. B 642 (2002) 290 [hep-lat/0205016]. For a more general review, see M.A. Stephanov, hep-ph/0402115.
12. D. Adamova et al. (CERES), Nucl. Phys. A 727 (97) 2003 [nucl-ex/0305002] and ref. therein.
13. J. Cleymans, R.V. Gavai, E. Suhonen, Phys. Rep. 130 (186) 217.
14. M.G. Alford, Nucl. Phys. Proc. Suppl. 117 (2003) 65 [hep-ph/0209287].
15. "Quark Matter 2004": <http://qm2004.lbl.gov/>. Proceedings of three most recent QM conferences: Nucl. Phys. A715 (2003); Nucl. Phys. A698 (2002); Nucl. Phys. A661 (1999).
16. C.A. Ogilvie, Nucl. Phys. A 698 (2002) 3c [nucl-ex/0104010]; M.A. Lisa, Nucl. Phys. A 698 (2002) 185c [nucl-ex/0104012].
17. U. Heinz, M. Jacob, nucl-th/0002042 and ref. therein.
18. L. McLerran, hep-ph/0202025; J.Nagle, T. Ullrich, nucl-ex/0203007; P. Jacobs, hep-ex/0211031; D. Kharzeev, Nucl. Phys. A 715 (441c) 2003 [nucl-th/0211083]; <http://www.bnl.gov/rhic/>
19. K. Kajantie, Nucl. Phys. A 715 (432c) 2003; P. Giubellino, Nucl. Phys. A 715 (441c) 2003; R.J. Fries, B. Müller, nucl-th/0307043.
20. http://www.gsi.de/zukunftsprojekt/index_e.html
21. J.D. Bjorken, Phys. Rev. D 27 (1983) 140.
22. K. Kajantie, L. McLerran, Ann. Rev. Nucl. Part. Sci. 37 (293) 1987; J.W. Harris, B. Müller, Ann. Rev. Nucl. Part. Sci. 46 (71) 1996 [hep-ph/9602235]; S.A. Bass, M. Gyulassy, H. Stöcker, and W. Greiner, J. Phys. G25 (1999) R1 [hep-ph/9810281].
23. T. Peitzmann and M.H. Thoma, Phys. Rep. 364 (2002) 175 [hep-ph/0111114].
24. R. Rapp, J. Wambach, Adv. Nucl. Phys. 25 (2000) 1 [hep-ph/9909229]; J.P. Wessels et al. (CERES), Nucl. Phys. A 715 (262c) 2003 [nucl-ex/0212015] and ref. therein.
25. J. Rafelski, J. Letessier, J. Phys. G 30 (2004) S1 [hep-ph/0305284]; R. Stock, hep-ph/0312039.
26. S.S. Adler et al. (PHENIX), Phys. Rev. Lett. 91 (072301) 2003 [nucl-ex/0304022], Phys. Rev. Lett. 91 (072303) 2003 [nucl-ex/0306021], nucl-ex/0308006; J. Adams et al. (STAR), Phys. Rev. Lett. 91 (172302) 2003 [nucl-ex/0305015], Phys. Rev. Lett. 91 (072304) 2003 [nucl-ex/0306024]; B.B. Back et al. (PHOBOS), Phys. Rev. Lett. 91 (072302) 2003 [nucl-ex/0306025]; I. Arsene et al. (BRAHMS), Phys. Rev. Lett. 91 (072305) 2003 [nucl-ex/0307003]; G. Agakichiev et al. (CERES), Phys. Rev. Lett. 92 (032301) 2004 [nucl-ex/0303014].
27. M. Asakawa, U. Heinz, B. Müller, Phys. Rev. Lett. 85 (2072) 2000 [hep-ph/0003169]; S. Jeon, V. Koch, Phys. Rev. Lett. 85 (2076) 2000 [hep-ph/0003168]; for a review, see: S. Jeon, V. Koch, hep-ph/0304012;

28. P. Braun-Munzinger, K. Redlich, J. Stachel, nucl-th/0304013.
29. J. Klay et al. (E895), Phys. Rev. C 68 (2003) 054905 [nucl-ex/0306033].
30. J. Barrette et al. (E877), Phys. Rev. C 51 (1995) 3309 [nucl-ex/9412003].
31. S.V. Afanasiev et al. (NA49), Phys. Rev. C 66 (2002) 054902 [nucl-ex/0205002].
32. I.G. Bearden et al. (NA44), Phys. Rev. C 66 (2002) 044907 [nucl-ex/0202019].
33. M.C. Abreu et al. (NA50), Phys. Lett. B 530 (2002) 33.
34. C. Oppedisano et al. (NA60), J. Phys. G 30 (2004) S507; G. Usai et al. (NA60), hep-ex/0307085.
35. B.B. Back et al. (PHOBOS), Phys. Rev. Lett. 88 (2002) 022302 [nucl-ex/0108009]; Nucl. Phys. A 715 (2003) 490c [nucl-ex/0211002].
36. S. Margetis et al. (NA49), Phys. Rev. Lett. 75 (1995) 3814; A. Bazilevsky (PHENIX), Nucl. Phys. A 715 (2003) 486c [nucl-ex/0209025].
37. K.J. Eskola, K. Kajantie, P.V. Ruuskanen, K. Tuominen, Nucl. Phys. B 570 (2000) 379 [hep-ph/9909456]; K.J. Eskola, K. Kajantie, K. Tuominen, Nucl. Phys. A 700 (2002) 509 [hep-ph/0106330].
38. C. Pinkenburg et al. (E895), Phys. Rev. Lett. 83 (1295) 1999; K. Filimonov et al. (E877), nucl-ex/0109017; K.H. Ackermann et al. (STAR), Phys. Rev. Lett. 86 (2001) 402; A.M. Poskanzer, nucl-ex/0110013; S. Voloshin, Nucl. Phys. A 715 (379c) 2003 [nucl-ex/0210014].
39. P.F. Kolb, U. Heinz, nucl-th/0305084.
40. U. Heinz, B.V. Jacak, Ann. Rev. Nucl. Part. Sci. 49 (529) 1999 [hep-ph/0204061]; B. Tomasik, U.A. Wiedemann, hep-ph/0210250.
41. M.A. Lisa et al. (E895) Phys. Rev. Lett. 84 (2798) 2000; D. Adamova et al. (CERES), Nucl. Phys. A 714 (124) 2003 [nucl-ex/0207005]; C. Adler et al. (STAR), nucl-ex/0107008; J. Adams et al. (STAR), nucl-ex/0312009; S.S. Adler et al. (PHENIX), nucl-ex/0401003.
42. D. Adamova et al. (CERES), Phys. Rev. Lett. 91 (042301) 2003 [nucl-ex/0207008].
43. P. Braun-Munzinger, J. Stachel, J. Phys. G 28 (2002) 1971.
44. A. Baran, W. Broniowski, W. Florkowski, nucl-th/0305075.
45. R. Stock, Phys. Lett. B 456 (1999) 277 [hep-ph/9905247].
46. P. Braun-Munzinger, J. Stachel, Ch. Wetterich, nucl-th/0311005.
47. F. Fecattini, Z. Phys. C 69 (1996) 485; F. Fecattini, U. Heinz, Z. Phys. C 76 (1997) 269.
48. L. Ahle et al. (E866/E917), Phys. Lett. B 476 (2000) 1 [nucl-ex/9910008]; L. Ahle et al. (E802), Phys. Rev. C 59 (1999) 2173.
49. S.S. Adler et al. (PHENIX), nucl-ex/0307022;
50. J. Adams et al. (STAR), nucl-ex/0311017. J. Adams et al. (STAR), nucl-ex/0310004.
51. L. Ahle et al. (E866/E917), Phys. Lett. B 490 (2000) 53 [nucl-ex/0008010].
52. C. Pinkenburg et al. (E895), Nucl. Phys. A 698 (2002) 495c [nucl-ex/0104025]; S. Ahmad et al. (E891), Nucl. Phys. A 636 (1998) 507 [nucl-ex/9803006]; T. Anticic et al. (NA49), nucl-ex/0311024; J. Adler et al. (STAR), Phys. Rev. Lett. 89 (2002) 092301 [nucl-ex/0203016].
53. P. Chung et al. (E895), Phys. Rev. Lett. 91 (2003) 202301 [nucl-ex/0302021]; S.V. Afanasiev et al. (NA49), Phys. Lett. B 538 (2002) 275; J. Adams et al. (STAR), nucl-ex/0307024.
54. M. Gaździcki, talk at "Quark Matter 2004"; P. Braun-Munzinger, talk at "Quark Matter 2004", <http://qm2004.lbl.gov/>.

55. E. Bratkovskaya et al., nucl-th/0401031.
56. T. Yamazaki et al., nucl-th/0310085.
57. M. Asakawa, T. Hatsuda, Phys. Rev. Lett. 92 (2004) 012001 [hep-lat/0308034]; P. Petreczky, S. Datta, K. Karsch, I. Wetzorke, hep-lat/0309012; H. Matsufuru, T. Umeda, K. Nomura, hep-lat/0401010.
58. E.V. Shuryak, G.E. Brown, Nucl. Phys. A 717 (2003) 322 [hep-ph/0211119].
59. P. Braun-Munzinger et al., Eur. Phys. J. C1 (1998) 123.
60. R. Gavai et al., Int. J. Mod. Phys. A 10 (1995) 3043 [hep-ph/9502270].
61. S.S. Adler et al. (PHENIX), hep-ex/0307019; H. Sato, hep-ph/0305239.
62. R. Vogt, hep-ph/0203151; hep-ph/0111271.
63. M.C. Abreu et al. (NA50), Nucl. Phys. A 698 (2002) 539c.
64. K. Adcox et al. (PHENIX), Phys. Rev. Lett. 88 (2002) 192303 [nucl-ex/0202002]; R. Averbeck (PHENIX) Nucl. Phys. A 715 (2003) 695c [nucl-ex/0209016].
65. M.C. Abreu et al. (NA50), Phys. Lett. B 450 (1999) 456; Phys. Lett. B 477 (2000) 28.
66. P. Crochet, Nucl. Phys. A 715 (359c) 2003 [nucl-ex/0209011].
67. M.C. Abreu et al. (NA50), Nucl. Phys. A 638 (1998) 261c; H. Santos (NA50), talk at "Quark Matter 2004", <http://qm2004.lbl.gov/>.
68. P. Braun-Munzinger, J. Stachel, Phys. Lett. B 490 (2000) 196 [nucl-th/0007059]; Nucl. Phys. A 690 (2001) 119c [nucl-th/0012064].
69. H. Sorge, E. Shuryak, I. Zahed, Phys. Rev. Lett. 79 (1997) 2775.
70. S.S. Adler et al., PHENIX Collaboration, nucl-ex/0305030.
71. A. Tai (STAR), talk at "Quark Matter 2004", <http://qm2004.lbl.gov/>.
72. M. Bedjidian et al., hep-ph/0311048; A. Dainese, nucl-ex/0312005.
73. R.L. Thews, M. Schroedter, J. Rafelski, Phys. Rev. C 63 (2001) 054905 [hep-ph/0007323]; R.L. Thews, hep-ph/0206179; R.L. Thews, hep-ph/0302050; R.L. Thews, hep-ph/0305316.
74. M.I. Gorenstein, A.P. Kostyuk, H. Stöcker, W. Greiner, Phys. Lett. B 509 (2001) 277 [hep-ph/0010148], Phys. Lett. B 524 (2002) 265 [hep-ph/0104071]; A.P. Kostyuk, M.I. Gorenstein, H. Stöcker, W. Greiner, Phys. Lett. B 531 (2002) 195 [hep-ph/0110269].
75. L. Grandchamp, R. Rapp, Phys. Lett. B 523 (2001) 60 [hep-ph/0103124], Nucl. Phys. A 709 (2002) 415 [hep-ph/0205305].
76. A. Andronic, P. Braun-Munzinger, K. Redlich and J. Stachel, Phys. Lett. B 571 (2003) 36 [nucl-th/0303036].
77. P. Braun-Munzinger and K. Redlich, Eur. Phys. J. C 16 (2000) 519.
78. M.I. Gorenstein, K.A. Bugaev, M. Gaździcki, Phys. Rev. Lett. 88 (2002) 132301 [hep-ph/0112197].
79. S. Batsouli, S. Kelly, M. Gyulassy, J.L. Nagle, Phys. Lett. B 557 (2003) 26 [nucl-th/0212068].
80. Yu.L. Dokshitzer, D.E. Kharzeev, Phys. Lett. B 519 (2001) 199 [hep-ph/0106202].
81. R. Vogt, Heavy Ion Phys. 9 (1999) 339 [nucl-th/9903051] and refs. therein. See also: D. Miśkowiec, <http://www.gsi.de/~misko/overlap/>.
82. J. Gosset, A. Baldisseri, H. Borel, F. Staley, Y. Terrien, Eur. Phys. J. C 13 (2000) 63.
83. R. Rapp, E. Shuryak, Phys. Lett. B 473 (2000) 13; K. Gallmeister, B. Kämpfer, O.P. Pavlenko, Phys. Lett. B 473 (2000) 20 [hep-ph/9908269].